Nuclear Materials and Energy 17 (2018) 48–55

Contents lists available at ScienceDirect

Nuclear Materials and Energy

journal homepage: www.elsevier.com/locate/nme

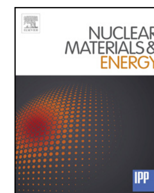

Study of the temperature-dependent nitrogen retention in tungsten surfaces using X-ray photoelectron spectroscopy

U. Plank*, G. Meisl, U. von Toussaint, T. Höschen, W. Jacob

Max-Planck-Institut für Plasmaphysik, Boltzmannstraße 2, Garching 85748, Germany

ARTICLE INFO

Keywords:
Plasma-wall interaction
Tungsten nitride
XPS quantification
Bayesian statistics
Sputter depth profiling
SDTrimSp
Ion-induced atom mobilisation

PACS:
28.52.Fa
52.40.Hf
79.20.Rf
79.60.Dp

ABSTRACT

Nitrogen is foreseen as seeding species in future magnetic confinement fusion reactors in order to reduce the power load from the plasma onto the divertor target tiles by radiative cooling. As a side effect it also gets implanted into the tungsten wall and forms tungsten nitrides (W_xN). The temperature-dependent W_xN formation was investigated in dedicated laboratory experiments. N ions of 300 eV kinetic energy were implanted into W samples under ultra-high vacuum conditions in the temperature range 300 K to 800 K. The N retention in W was monitored and quantitatively analysed by X-ray photoelectron spectroscopy (XPS). A method to calculate the statistical error of the measured data based on Bayesian statistics was developed. Argon sputter depth profiling was combined with XPS to measure N in W depth profiles which were compared with simulated N implantation profiles. Annealing of samples implanted with N at 300 K does not cause a loss of N up to 800 K. However, the retained N amount decreases linearly with increasing implantation temperature. It was found that this reduction is due to ion-irradiation-induced N release at elevated temperatures. Over the whole temperature range N diffusion into depth was not observed. N accumulation measurements showed no evidence for a phase transition in the W_xN layer. However, high resolution XPS measurements revealed that below 600 K a second photoelectron peak occurs in the N 1*s* signal which can be attributed to different local atomic arrangements of W_xN.

1. Introduction

In magnetically confined fusion plasmas, the magnetic field configuration must be chosen in a way that minimizes the interaction of the plasma with the surrounding vessel wall. In the divertor configuration the inner field lines are closed in order to confine the plasma, but the outermost magnetic field lines intersect the wall. They intentionally lead expelled plasma particles onto a small region of the vessel wall remote from the plasma, the divertor. The favoured material for the divertor tiles is tungsten (W), since its erosion and hydrogen retention is low [1]. The thermal loads onto the divertor in future fusion reactors can, however, easily exceed the power handling capabilities of tungsten [1,2]. For this reason, seeding of impurity gas in the divertor region is necessary. The seeded gas particles get ionised by the plasma particles, emit line radiation homogeneously in all directions and, therefore, reduce the power load onto the divertor target tiles. Nitrogen (N) as seeding species is a promising candidate [2]. However, the energetic nitrogen species can on the one hand increase the W sputtering of the chamber wall and on the other hand get implanted into the W tiles and form tungsten nitrides (W_xN). This might lead to a competition between W_xN formation and W erosion depending on the influxes and the impurity composition. For a better understanding of the W_xN formation and N retention in W under reactor relevant conditions, laboratory experiments employing X-ray photoelectron spectroscopy (XPS) were conducted. The obtained results are compared with findings from [3], [4] and [5], which are briefly described here: In [3] the interaction of pure N plasmas with magnetron-sputter-deposited W films was investigated. The W samples were exposed to N ions from a low-temperature plasma source with energies ranging from 20 eV to 500 eV at a temperature of about 350 K. It was found that N accumulation in W is limited at this temperature to the implantation zone. This is attributed to the low diffusivity of N in W. In an other experiment described in [3] bulk W samples were implanted with N in a plasma-immersion-ion-implantation device, applying a pulsed implantation voltage of 10 keV. The N content in W decreased with increasing implantation temperature, which ranged from 600 K to 750 K. XPS measurements of the W 4*f* signal of N-implanted W samples revealed that the W_xN peak is shifted to higher binding energies (BEs) for an implantation temperature of 800 K compared with the W_xN peak of N implantation at 300 K or 600 K. It was also found that the investigated photoelectron signal of the N 1*s* orbital consists of more than one peak, indicating different local atomic arrangements of the bound N. These observations are in

* Corresponding author.
E-mail address: Ulrike.Plank@ipp.mpg.de (U. Plank).

https://doi.org/10.1016/j.nme.2018.08.006
Received 24 June 2018; Received in revised form 24 August 2018; Accepted 25 August 2018
2352-1791/ © 2018 The Authors. Published by Elsevier Ltd. This is an open access article under the CC BY-NC-ND license
(http://creativecommons.org/licenses/BY-NC-ND/4.0/).

agreement with thermodynamic calculations which predict a phase change of WN to W_2N at about 600 K [3]. On the other hand, temperature-dependent N desorption measurements of magnetron-sputtered W_xN films in [5] showed that W_xN decomposes only above 830K. The desorption spectrum consists of two release peaks with their maxima at 925 K and 960 K. In [4] W_xN layers were created by implanting N ions of 2.5 keV kinetic energy into W. The W_xN formation was followed by XPS. It was found that no measurable amount of N is lost from the surface while heating the W_xN sample up to 800 K. However, the N retention in the W sample decreased when N was implanted at 500 K and 800 K sample temperature.

The aim of this study is a more detailed evaluation of the N retention in W, i.e. the N accumulation in W and the N release from W_xN, in the temperature range 300 K to 800 K. Fluence series of N_2^+ ions impinging with 300 eV per atom on a W sample were acquired. The relative N concentration in the surface was determined by quantitative analysis of the measured XPS spectra. Additionally, a method based on Bayesian statistics was developed in order to calculate the statistical error of the measurements. Sputter depth profiles employing Ar ions of 1 keV kinetic energy were acquired and, together with SDTrimSP simulations, used to determine the N depth distributions.

2. Methods

2.1. Experimental procedure

The W samples employed in the experimental study were hot-rolled W plates with a purity of 99.97 mass percent. The samples are identical to those used in [4]. Before usage the W samples were ground, polished and annealed at 1200 K under vacuum conditions for two hours to guarantee a clean and smooth surface [6].

Sample preparation and analysis was performed in a commercial XPS device, a PHI ESCA 5600. The base pressure in the main vacuum chamber was below 1.5×10^{-10}mbar. The samples can be heated up to 900 K from the bottom side using a tantalum filament mounted on the specimen holder. A thermocouple is attached to the specimen holder next to the sample in order to measure and control the sample temperature. N was implanted in situ into the W samples using a Wien-filtered SPECS IQE 12/38 ion source. It is mounted at an angle of 45° to the sample surface. The ion source was operated with an acceleration voltage of 600 V and produced a beam of N_2^+ ions. Therefore, the energy per N atom was 300 eV. This energy was chosen since it is close to the predicted upper limit of the ion impact energy with which N ions from the edge plasma collide with the chamber wall [7]. Lower N ion energies could not be used, because space-charge effects become dominant, which lead to an increase of the ion beam diameter and to a strong reduction of the local ion flux. A second SPECS IQE 12/38 ion source without Wien mass filter producing Ar ions of 1 keV kinetic energy was used for cleaning the W surface from surface oxides and adsorbates prior to N implantation. The Ar ion beam was also applied after N implantation to stepwise remove the formed W_xN surfaces for sputter depth profiling. Alternating to the sputter intervals XPS spectra were acquired to determine the N content in W as a function of the accumulated Ar fluence. The sputter yield for Ar ions impinging at an angle of 40° to the surface is about 1.3 [8]. An Ar fluence of $1 \times 10^{20}\,\mathrm{m}^{-2}$, therefore, sputters approximately 2 nm of pure W. The ion fluence was determined by measuring the sample current. Previous experiments from [4] have shown that under the present implantation conditions secondary electrons account for about 10% of the measured current. This amount was subtracted from the sample current.

To attain homogeneous ion irradiation on the sample the N ion beam was rastered over an area of 5 mm × 5 mm and the Ar beam over 4.5 mm × 4.5 mm. Both ion beams have a Gaussian profile with a full width at half maximum (FWHM) of 0.8 mm for the N beam and 1.5 mm for the Ar beam. The actually irradiated area was determined to be 33 mm^2 for the N and 36 mm^2 for the Ar beam. This leads to a mean N ion flux of about $3.6 \times 10^{16}\,\mathrm{s}^{-1}\mathrm{m}^{-2}$ and to a mean Ar flux of $9.5 \times 10^{16}\,\mathrm{s}^{-1}\mathrm{m}^{-2}$ on the target.

During the acquisition of XPS spectra the ion bombardment was stopped, while the heating of the sample, if applied, was continued. Since residual gas may adsorb on the surface during acquisition, the acquisition time of the XPS spectra was chosen as short as possible. To still have a high count number, the acquisition was restricted to the N 1*s*, W 4*f*, carbon and oxygen photoelectron peaks. This led to an acquisition time of 5 to 15 min, depending on the quality of the N 1*s* photoelectron signal. The acquisition time was increased to 30 min for high-resolution spectra. Monochromatic X-rays were produced with an aluminium (Al) anode X-ray source plus monochromator. This radiation has an energy of 1486.7 eV and a FWHM of 0.50 eV. Due to technical problems the X-ray source with monochromator could not be used for all measurements. The Al K_α-line of a dual-anode source was used instead, which has a FWHM of 0.85 eV. A N implantation experiment at 300 K employing both sources showed that the use of the non-monochromated X-ray radiation does not change the intensity ratio of the measured N 1*s* to W 4*f* peaks.

The emerging photoelectrons entered the analyser with multichannel detector via an OmniFocus III lens system. The lens system decelerates the electrons to the pass energy of the analyser. The hemispherical energy analyser is positioned at 45° to the sample surface and at 90° to the monochromatic X-ray source. The angle between the analyser and the dual-anode X-ray source is 54.7°. The pass energy of the analyser was constant and chosen to 93.9 eV in order to have a high count rate. For high resolution measurements the pass energy was set to 11.75 eV with a reduction of the lens system's aperture from 1.1 mm to 0.6 mm.

2.2. Quantitative analysis of XPS spectra

Quantitative analysis of XPS spectra means to determine the depth-dependent particle density $n_A(z)$ of element A within the depth of three to five electron's inelastic mean free paths. The XPS signal is an exponentially weighted average over this depth [9]. The area I_A under the photoelectron peak of element A can be calculated to

$$I_A = \sigma_A\, L_A\, T(E)\, \Gamma_{\mathrm{phot}}\, t \int_0^\infty n_A(z) \exp\left(-\int_0^z \frac{1}{\lambda(z')\cos\alpha} \mathrm{d}z'\right) \mathrm{d}z, \tag{1}$$

with σ_A, the total cross section, L_A, the angular asymmetry of the studied orbital, $T(E)$, the transmission function of the analyser, which also depends on the photoelectron's energy E, Γ_{phot}, the incoming photon flux, t, the acquisition time, $\lambda(z')$, the electron's inelastic mean free path in the depth z', and α, the angle between detector and sample normal [4,10].

The background which was subtracted from each photoelectron peak consists of a constant part s^0 and a contribution which arises due to inelastic scattering of the photoelectrons. To account for the latter, the commonly used Shirley background was calculated [11]. If s_i is the actual photoelectron signal, i.e. the background subtracted signal of channel i, then the Shirley background of s_i is $k\sum_{j=1}^{i-1} s_j$ with the fit parameter $k \in [0, 1]$. The Shirley background was calculated for the measured N 1*s* and W 4*f* signals using the XPS data processing program MultiPak version 9.0. The integration limits were set to 393 eV and 405 eV for the N 1*s* peak and to 26 eV and 44 eV for the W 4*f* peak. To determine the N 1*s* to W 4*f* intensity ratio, the background-subtracted photoelectron peak signals were integrated over the full measured range and divided. The intensity ratio is a quantity which is independent of set-up-dependent factors as, e.g., the incoming photon flux. For comparison of the measured intensity ratios with simulations not the Shirley background, but the Tougaard background has to be calculated. The Tougaard background is based on a physical model employing a universal cross section for inelastic scattering instead of the fit parameter k [10]. According to [4] the calculated N 1*s* to W 4*f*

intensity ratio is corrected for the Tougaard background by multiplying it with a factor of 1.42.

2.3. Statistical error calculation

The detected signal d_i of channel i ($i = 1...N$, N: total number of channels) obeys counting statistics, i.e. a Poisson distribution. This converges for a large number of counts to a Gaussian distribution, i.e. $p(d_i) = \mathcal{N}(d_i, \sqrt{d_i})$.

For the calculation of the statistical error of the photoelectron signal a Bayesian approach is used, since the underlying background depends itself on the signal intensity (see Section 2.2). For this approach the region around the XPS peak of interest was split into three distinct parts with different properties. In the first part (this is at lower BEs than the peak of interest) only a constant background s^0 is apparent. In the second part (i.e. the peak of interest) the signal of each channel is the sum of s^0, the actual photoelectron signal s_i and the Shirley background $k\sum_{j=1}^{i-1} s_j$. The signal in the third part (i.e. at higher BEs than the peak of interest) consists of the constant background s^0 and the Shirley background.

Using vector notation, the detected signal $\boldsymbol{d} = (d_1, ..., d_N)$ can be written as

$$\boldsymbol{d} = \boldsymbol{M}(k)\boldsymbol{s} + \boldsymbol{\sigma}, \quad (2)$$

$$\text{with} \quad \boldsymbol{M}(k) = \begin{pmatrix} 1 & 1 & 0 & 0 & \cdots \\ 1 & k & 1 & 0 & \cdots \\ \vdots & \vdots & & \ddots & \\ 1 & k & k & \cdots & 1 \end{pmatrix}, \quad \boldsymbol{s} = (s^0, s_1, ..., s_N), \quad \boldsymbol{\sigma} = (\sqrt{d_1}, ..., \sqrt{d_N})$$

and k the fitting parameter of the Shirley background. To determine the probability distribution of the photoelectron signal, $p(\boldsymbol{s}, k|\boldsymbol{d})$, Bayesian statistics is used [12]. The prior probability $p(\boldsymbol{s}, k)$ is assumed to be positive and constant. Due to the Gaussian distribution of the detected signal of each channel, the likelihood $p(\boldsymbol{d}|\boldsymbol{s}, k)$ can be written as a multivariate Gaussian distribution, i.e. $\mathcal{N}(\boldsymbol{y}, \boldsymbol{C} = \text{diag}(d_1, ..., d_N))$. It turns out that the posterior probability $p(\boldsymbol{s}, k|\boldsymbol{d})$ is sharply peaked around one value, $\hat{k}$. Therefore, it is possible to marginalise over k with negligible error using the peak approximation for k. This results in a multivariate Gaussian distribution with

$$p(\boldsymbol{s}|\boldsymbol{d}, \hat{k}) = \mathcal{N}((\boldsymbol{M}^\intercal(\hat{k})\boldsymbol{C}\boldsymbol{M}(\hat{k}))^{-1}\boldsymbol{M}^\intercal(\hat{k})\boldsymbol{C}\boldsymbol{d}, (\boldsymbol{M}^\intercal(\hat{k})\boldsymbol{C}\boldsymbol{M}(\hat{k}))^{-1}). \quad (3)$$

Eventually, we are interested in the integral of the photoelectron signal s_i over all channels i and its uncertainty. The integral of a multivariate Gaussian can be expressed as a linear combination of its components. This allows for an analytical formulation of the statistical error of the peak area.

The statistical error of the N 1s peak was calculated with the first region ranging from 393 eV to 395 eV, the second region from 395 eV to 402 eV and the third region from 402 eV to 405 eV. The statistical error of the W 4f peak was found to be negligible and, therefore, not taken into account.

2.4. Simulations

2.4.0.1. SDTrimSP. SDTrimSP is a Monte Carlo code which simulates the interaction of energetic particles with matter based on the binary collision approximation [13]. The N depth distribution shown in Fig. 1 (solid line) was simulated with the dynamical mode of SDTrimSP version 5.00. In this simulation it was assumed that N atoms impinge with 300 eV kinetic energy on a W target under an angle of 45°. The surface binding energy of N in W was set to 0.1 eV and the maximum N concentration to 50% [14].

2.4.0.2. Forward Calculation. As can be seen from Eq. (1) it is not possible to calculate the actual depth distribution from intensity ratios. This implies that the N depth distribution obtained from SDTrimSP simulations and the sputter depth profile, i.e. the XPS intensity ratios measured as function of the Ar fluence, can not be compared directly. However, it is possible to convert the N depth distribution simulated by SDTrimSP into XPS intensity ratios via forward calculation [4]. The output of SDTrimSP is given in discrete depth layers l of thickness Δx_l with a homogeneous particle density $n_{A,l}$. The outgoing intensity of element A, I_A, can be calculated using the Beer-Lambert law [9]:

$$I_A = \xi_A \sum_l n_{A,l}\lambda_l \left(1 - \exp\left(\frac{-\Delta x_l}{\lambda_l}\right)\right) \exp\left(-\sum_{j=0}^{l-1} \Delta x_j/\lambda_j\right), \quad (4)$$

with ξ_A, a pre-factor containing the total cross section and the angular asymmetry and λ_l, the inelastic mean free path in layer l. The cross sections used for the calculation are taken from [15], the asymmetry parameters from [16] and the inelastic mean free path from [17]. The depth profile calculated from the simulated N depth distribution is shown as dashed line in Fig. 1.

3. Results and discussion

3.1. Sample annealing after N implantation at 300 K

It was found in [4] that W_xN layers created by N implantation into bulk W do not decompose up to 800 K and this observation is in agreement with the thermal desorption results reported in [5]. Since in the present study N ions with 300 eV kinetic energy were used, the total N amount in the sample is lower than that in [4] which used N ions of 2.5 keV kinetic energy. To check whether W_xN formed by irradiation with 300 eV N ions shows a comparable thermal stability, N was implanted into a W sample at 300 K until a steady-state N 1s to W 4f intensity ratio, i.e. saturation was reached. Saturation was reached after six hours which corresponded to a N fluence of $6 \times 10^{20} \text{m}^{-2}$. After implantation the sample was heated to 800 K and held at this temperature for 5 h. Fig. 2 shows the N 1s to W 4f intensity ratios (squares) measured before and during annealing together with the temperature (solid line) as a function of annealing time. The first data point represents the saturated N 1s to W 4f intensity ratio just before starting the heating ramp. Heating to 800 K took about 30 min. The next data point was measured directly after reaching 800 K. The following three data points were measured after various holding times up to 5 h. The data points scatter around a constant value of 0.16 (dashed line). However, no decrease in the intensity ratios is visible within the statistical error which confirms that the formed W_xN does not decompose during annealing at 800 K on a time scale of several hours. In this measurement, the pass energy of the analyser was set to 11.75 eV. Since the transmission function of the analyser depends on the pass energy [9], the values of the intensity ratios differ from the values obtained in the follow-up experiments, where a pass energy of 93.9 eV was chosen. Furthermore, the statistical error was not calculated as described in Section 2.3, but experimentally determined. A second W sample was implanted with N at 300 K and held at this temperature for several hours. XPS spectra were acquired after different holding times and the scatter in the calculated N 1s to W 4f intensity ratios taken as the statistical error. The so-determined statistical error of the intensity ratio is ± 5%.

The sputter depth profile which was acquired after the annealing procedure is shown as squares in Fig. 3. Also shown in Fig. 3 is the reference (circles), a sputter depth profile of a W_xN sample where N was implanted at 300 K without subsequent annealing. For the acquisition of the reference spectrum the dual-anode X-ray source was used, which, in our experiments, had no influence on the measured XPS intensity ratios. The two sputter depth profiles shown in Fig. 3 were measured at 300 K sample temperature. Both start at a comparable intensity level which decreases with the same rate with increasing Ar fluence, i.e. with depth. From this we conclude that neither the N content in the sample nor the N depth distribution change due to the annealing process.

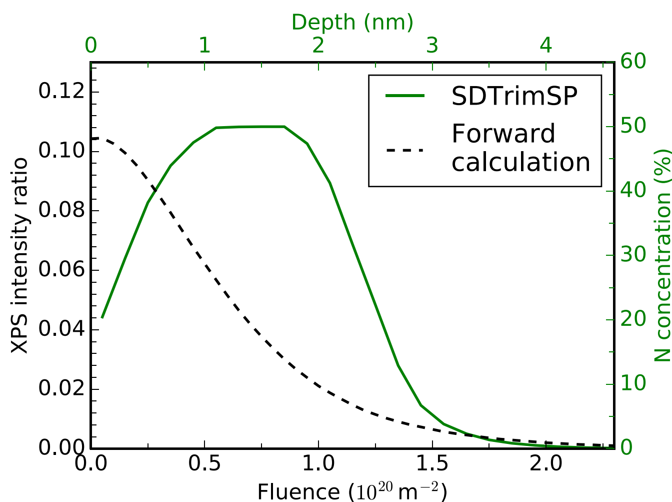

Fig. 1. Conversion of a depth distribution into an XPS depth profile. The solid line represents the depth distribution of N atoms impinging with 300 eV kinetic energy on a W target simulated with SDTrimSP version 5.00. The XPS depth profile (dashed line) is obtained from the simulated N depth distribution via forward calculation (see Section 2.4).

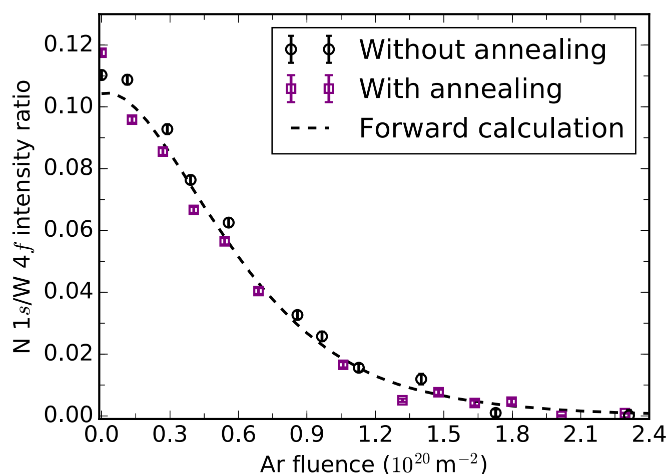

Fig. 3. Two sputter depth profiles of W_xN samples measured at 300 K. N was implanted at 300 K in both samples. One sample (squares) was annealed at 800 K for 5 h after implantation, the other sample (circles) was not annealed. The error bars indicate the calculated statistical error (see Section 2.3). The dashed line represents the depth profile calculated from the SDTrimSP N depth distribution (see Fig. 1).

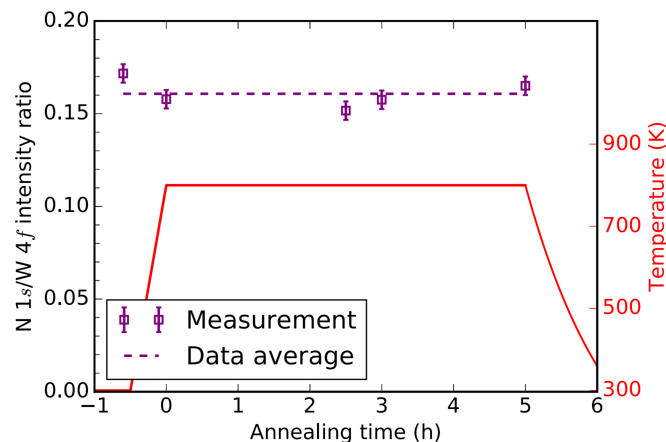

Fig. 2. Annealing of a W sample after N implantation: The N 1*s* to W 4*f* intensity ratios (squares) were measured on a W sample which was implanted with N at 300 K and subsequently annealed at 800 K for 5 h. The measurements were acquired with an analyser pass energy of 11.75 eV. The error bars represent the experimentally determined statistical error (for details see Section 3.1). The dashed line is the average of all five data points. The solid line represents the temperature evolution during the experiment.

Obviously the formed W_xN phase is, at 800 K, thermally stable on a time scale of several hours.

The two sputter depth profiles are also compared with the calculated depth profile (dashed line) from the SDTrimSP simulation (see also Fig. 1), which shows the same behaviour as the measured profiles. The good agreement of the measured data with the calculated intensity ratios implies that N implantation in W at 300 K can be simulated by SDTrimSP. It also supports the conclusion that the N depth distribution does not change due to heating the sample to 800 K.

3.2. N implantation in temperature range 300 K to 800 K

N accumulation in the W surface as a function of N fluence was investigated at different implantation temperatures ranging from 300 K to 800 K. The measured N 1*s* to W 4*f* intensity ratios are shown in Fig. 4. The experiment was conducted in the following way: At a given temperature N was implanted into the sample up to a certain N fluence. Then N implantation was suspended and XPS spectra were acquired. After that the N implantation was continued up to the next N fluence step. During the whole procedure the sample was kept at the corresponding temperature. It takes about 22 h to accumulate the highest here investigated N fluence of $17 \times 10^{20}\,\mathrm{m}^{-2}$. The integrated XPS measuring time for the three temperature series measured at 300 K, 400 K and 500 K varies between 70 min and 150 min. This means that the total holding time of the samples at the given temperature is 4.5% to 25% longer than the pure implantation time. We emphasize, however, that we found no indication of N loss during the XPS measuring periods.

At 800 K two fluence series were measured. In the first experiment (squares) the sample contained about 4% of N already before the N implantation was started. This corresponds to a N 1*s* to W 4*f* intensity ratio of about 0.01 and was caused by a N contaminated Ar beam, which was applied for cleaning the surface from adsorbates prior to the N implantation. For this reason the spectra at low fluence, where the N content is dominated by the initial N contamination, were discarded. As will be shown later in Fig. 8, samples with pre-existing W_xN reach the same steady-state XPS intensity ratio at a given sample temperature as samples with no pre-existing W_xN. Therefore, the data measured at high N fluence (squares) are shown in Fig. 4 in order to determine the saturation level. The N 1*s* to W 4*f* intensity ratios at 800 K at low N fluence (triangles) were measured in a second N implantation, starting with a N-free surface. The saturation levels at 700 K and 600 K originate from a different N implantation experiment in which the temperature was decreased in steps of 100 K from 800 K to 300 K. At each temperature step N implantation was continued until a steady-state intensity ratio was reached. Hence, no comparable fluence series as for the other temperatures shown in Fig. 4 are available for these two temperatures. Additionally, the equilibrium levels for 600 K and 700 K as they were obtained in the experiment described in Section 3.3 are shown as dashed lines in the figure. The data of the first implantation at 800 K (squares) as well as the data of the fluence series at 300 K (circles) were acquired with the dual-anode X-ray source. This has, as stated before, in our experiment no influence on the measured N 1*s* to W 4*f* intensity ratios.

As can be seen in Fig. 4, the N 1*s* to W 4*f* intensity ratio increases at all investigated implantation temperatures initially steeply, then it flattens and finally reaches a temperature-dependent steady-state intensity ratio, i.e. its saturation level. The dependence of the N 1*s* to W 4*f* intensity ratio y on the fluence x can be described by a saturation curve

Table 1
Saturation level c and growth constant x_0 of N implantations in W at different temperatures determined by least-square fits of Eq. (5) to the experimental data (see Fig. 4).

Temperature (K)	Saturation level c	Growth constant x_0 (10^{20}m^{-2})
300	0.11	2.5
400	0.089	2.4
500	0.076	2.3
600	0.051	not determined
700	0.029	not determined
800	0.023	0.53

$$y(x) = c\left(1 - \exp\left(-\frac{x}{x_0}\right)\right), \tag{5}$$

with c, the saturation level and x_0, the growth constant. Both values were determined by least-square fits to the experimental data and are listed in Table 1. The growth constant x_0 decreases slightly with implantation temperature for the fluence series measured at 300 K, 400 K and 500 K, but it is about a factor of 5 smaller for the implantation at 800 K. The saturation level c decreases linearly with implantation temperature as shown in Fig. 5. This observation cannot easily be reconciled with the occurrence of a phase change from WN to W_2N at about 600 K as it was suggested in [3]. In such a case a significant jump of the steady-state intensity ratio around the phase transition temperature would be anticipated. However, the reduction of the saturation level with increasing implantation temperature implies that the N inventory in the surface of the W sample decreases. In the following, sputter depth profiles were measured for these samples to clarify whether N effuses from the surface at increased temperatures or if it diffuses into larger depth of the W sample, out of the XPS detection range.

The sputter depth profiles of the N implantations at 500 K (diamonds) and 800 K (triangles) are shown in Fig. 6 (a) together with the sputter depth profile of the N implantation at 300 K (circles). The latter is identical to the reference sputter depth profile shown in Fig. 3. All three profiles were measured at 300 K. The two depth profiles of N implantation at increased temperature decrease fast with increasing Ar fluence and drop to zero at an Ar fluence of about 1.5×10^{20} m^{-2}. This fluence roughly corresponds to a depth of 2.7 nm. The intensity ratio of

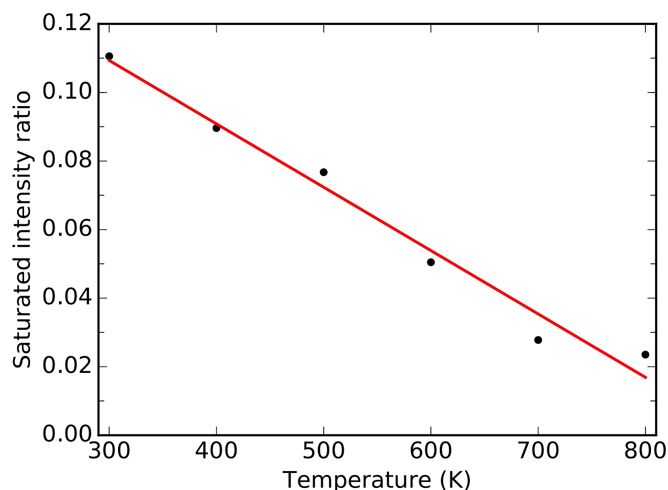

Fig. 5. Plot of the saturation level from Fig. 4 (see also Table 1) as a function of the implantation temperature. The solid line is a linear fit to the data points.

the N implantation at 300 K stays constant up to an Ar fluence of 0.2×10^{20} m^{-2} before it decreases and drops to zero at an Ar fluence of about 1.7×10^{20} m^{-2}. The observation that the signal of all three depth profiles vanishes at similar Ar fluences leads to the conclusion that under the described conditions implanted N is only present in W in the first 2–3 nm and does not diffuse into larger depth at increased temperature.

For further interpretation of the three measured sputter depth profiles they are compared with depth profiles calculated from three different modeled N depth distributions. The calculated depth profiles are shown as dashed, dotted and solid lines in Fig. 6 (a) while their underlying N depth distributions are shown in Fig. 6 (b). The underlying N depth distribution of the reference depth profile (dashed line) is the simulated SDTrimSP distribution from Section 2.4. Since SDTrimSP is a collision-based code to simulate the interaction of energetic particles with matter it does not include composition changes of the target due to temperature effects. In order to extract the quantities which mainly change when irradiating a W sample with N ions at elevated temperatures, simple model N depth distributions were chosen as underlying N depth distributions which resemble the SDTrimSP simulated

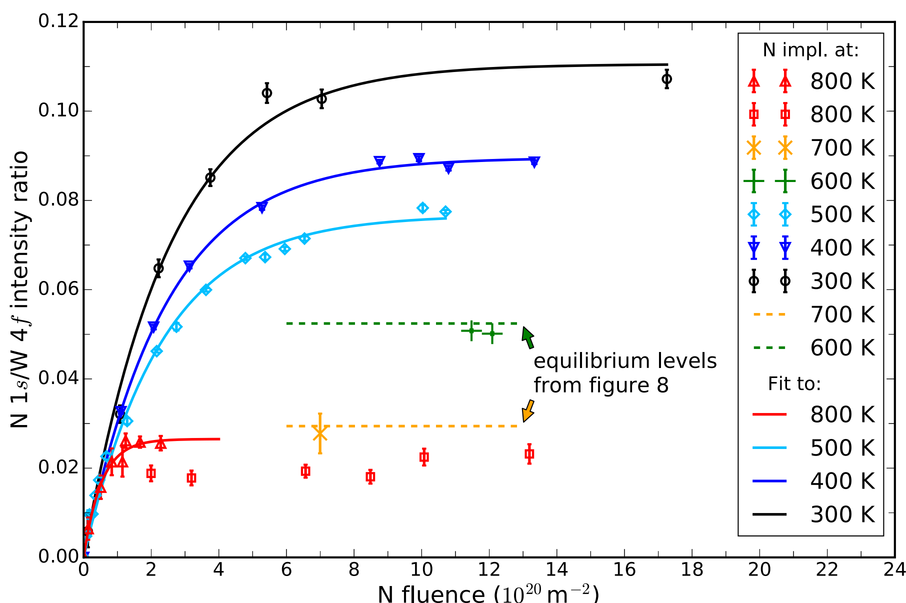

Fig. 4. N accumulation at different implantation temperatures: The N 1s to W 4f intensity ratios were measured as a function of the N fluence until they saturated (for details see text). The error bars represent the calculated statistical error. Solid lines are least-square fits to the data according to Eq. (5).

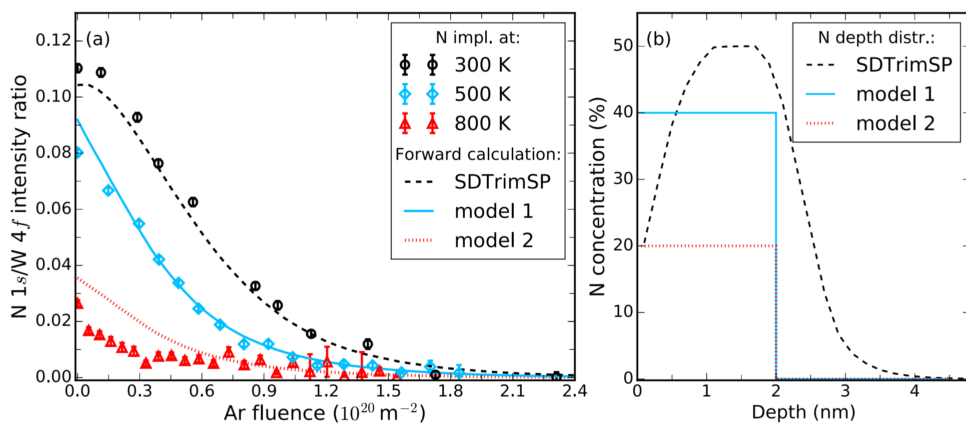

Fig. 6. (a) Sputter depth profiles measured at 300 K of N implantations in W at 300 K, 500 K and 800 K sample temperature. The error bars indicate the calculated statistical error. The three lines in the figure represent depth profiles determined by forward calculation (see Eq. (4)) from three different N depth distributions shown in (b). (b) A N depth distribution as it was simulated for 300 eV N atoms on W with SDTrimSP version 5.00 (see also Fig. 1) and two model N distributions, where a step-function profile was assumed with 40% N (model 1) and 20% N (model 2) in the first 2 nm, respectively.

depth distribution in terms of N implantation depth, but have a reduced maximal N concentration. For these step function N depth distributions it was assumed that N is present in the first 2 nm with 40% (solid line) and 20% (dotted line), respectively. Obviously, the sputter depth profile of the N implantation at 500 K (diamonds) and the calculated depth profile of the N depth distribution with a N concentration of 40% (solid line) are in good qualitative and quantitative agreement. This indicates that the underlying N depth distribution for N implanted in W at 500 K looks similar to the model distribution and the maximal N concentration is reduced from 50% to about 40%. The calculated depth profile of the N depth distribution with 20% N (dotted line) agrees with the sputter depth profile of the N implantation at 800 K at an Ar fluence larger than $0.5 \times 10^{20}\,\mathrm{m}^{-2}$. At an Ar fluence smaller than $0.5 \times 10^{20}\,\mathrm{m}^{-2}$ the measured N 1*s* to W 4*f* intensity ratios are lower than the calculated N 1*s* to W 4*f* intensity ratios. This indicates that close to the surface the actual N depth distribution differs from the assumed model N depth distribution and the N concentration in this depth is even lower than 20%. From the comparisons of the simulations with the measurements we conclude that the higher the N implantation temperature is the lower is the overall N concentration in the W sample, but N does not diffuse into depth.

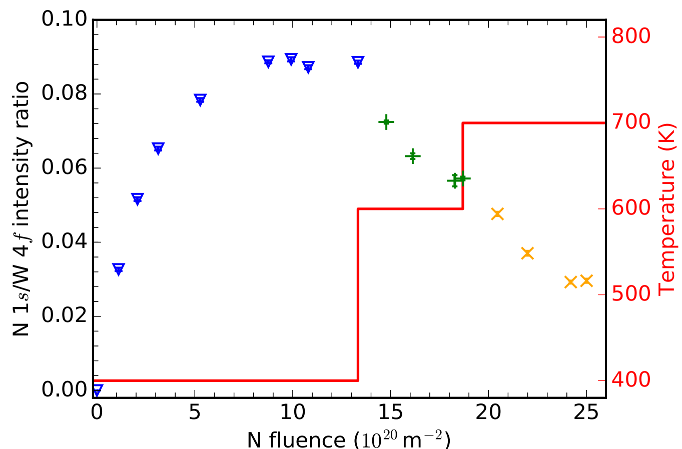

Fig. 8. N release by N irradiation: N was implanted into a W sample at 400 K (triangles) until saturation was reached. Subsequently, the sample was heated to 600 K (green crosses) and the N implantation was continued until a steady-state intensity ratio was reached. The same was done at 700 K (orange crosses). The solid line indicates the temperature profile. The N 1*s* to W 4*f* intensity ratios at 400 K are the identical data shown in Fig. 4. (For interpretation of the references to colour in this figure legend, the reader is referred to the web version of this article.)

High Resolution XPS Measurements. High resolution XPS spectra of the saturated W 4*f* and N 1*s* peak were acquired during the experiment where the temperature was stepwise decreased from 800 K to 300 K. The corresponding peak spectra are shown in Fig. 7 (a) and 7 (b), respectively. For a comparison the W 4*f* peak of pure tungsten, which was acquired before implantation was started, is also shown in Fig. 7 (a). The W 4*f* peak after N implantation at 800 K is in width and height very similar to the W 4*f* peak of pure tungsten. The only difference is a small broadening towards higher BE. With decreasing implantation temperature the W 4*f* peak height decreases and the peak broadens more towards higher BE. This broadening is a superposition of one or more W_xN peaks emerging at higher BEs than the pure W peak and

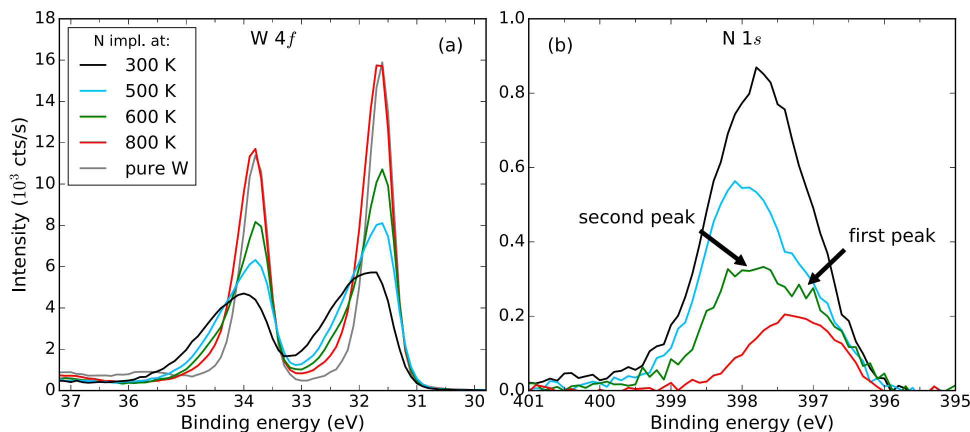

Fig. 7. High resolution XPS measurements of the W 4*f* (a) and N 1*s* (b) signals: The sample temperature was stepwise decreased from 800 K to 300 K and N was implanted at each temperature step. The spectra were acquired after the steady-state N 1*s* to W 4*f* intensity ratio was reached.

shows that more W_xN is formed at lower implantation temperature. Accordingly, the N 1*s* signal in Fig. 7 (b) becomes more intense with decreasing implantation temperature. At 800 K the N 1*s* signal consists of one peak with the maximum at around 397.2 eV. At 600 K a second peak at 398 eV appears. This leads between 500 K and 300 K to an asymmetric N 1*s* signal consisting of more than one peak, as it was already reported in [3]. The occurence of several N 1*s* peaks at different BEs is the consequence of different local atomic arrangements of the N atoms in the W lattice [9]. A possible explanation is that at low implantation temperatures different W_xN phases emerge in the sample while at high temperatures only one phase is present. According to the phase diagram in [3] this would mean that at low implantation temperatures the WN and the W_2N phases develop while at implantation temperatures above 600 K only the W_2N phase emerges.

3.3. Impact of temperature on N release under ion irradiation

N Release under N Ion Irradiation. Fig. 8 shows the evolution of the N content in W_xN layers under N irradiation with simultaneous sample temperature changes. In this experiment N was implanted into W at 400 K (triangles) until saturation. Subsequently, the sample was heated to 600 K (green crosses) and later to 700 K (orange crosses). As the new sample temperature was reached the N irradiation was continued until again a steady-state intensity ratio was reached. The data in Fig. 8 show that after an increase of the sample temperature the N 1*s* to W 4*f* intensity ratio decreases with increasing N fluence until the new equilibrium level is reached. This new equilibrium level depends on the implantation temperature and is comparable to the saturation level obtained from the N implantation at 600 K and 700 K, respectively (see Fig. 4). In contrast to the findings from Section 3.1, where the experiment showed that W_xN does not decompose up to 800 K, the additional N irradiation paradoxically leads to a loss of N from the surface already below 800 K. Furthermore, the amount of released N increases with increasing temperature.

N Release under Ar Ion Irradiation. In the next experiment it was investigated if Ar ion irradiation at elevated temperature also leads to an enhanced N release from W_xN. A well known mechanism resulting in temperature dependent erosion rates is chemical erosion and Ar does not chemically interact with the W_xN system [18].

N was implanted at 300K until the saturation level was reached. Afterwards the W_xN sample was heated to 800 K. The heating process took about 30 min. As soon as this temperature was reached, irradiation of the sample by Ar ions was started and between the irradiation steps XPS spectra were acquired. The measured N 1*s* to W 4*f* intensity ratios are shown as triangles in Fig. 9. For comparison, the N 1*s* to W 4*f* intensity ratios of Ar sputtering at 300 K (circles) are shown. They were already presented in Figs. 3 and 6. The N 1*s* to W 4*f* intensity ratio measured at 800 K stays constant up to an Ar fluence of $0.2 \times 10^{20}\,m^{-2}$. Above this value the N 1*s* to W 4*f* intensity ratio decreases rapidly with Ar fluence and drops to zero at about $0.7 \times 10^{20}\,m^{-2}$. The N erosion rate at 800 K is more than a factor of two higher compared to the erosion at 300 K (see dashed line in Fig. 9). This observation shows that enhanced N release at elevated temperature can be also induced by Ar ion irradiation and leads to two conclusions: Firstly, ion irradiation can induce thermal N release from W_xN already below 800 K and the N release is not caused by chemical erosion. Secondly, the N release under ion irradiation is temperature-dependent and it increases with increasing sample temperature.

Based on the conducted experiments the following picture emerges: Energetic particles penetrating into W_xN deposit energy within their penetration depth and may also break existing W_xN bonds on their way into the bulk, thus producing unbound N atoms. The mobility of the unbound N atoms increases with increasing temperature and, hence, the migration of the N atoms via interstitial sites to the surface.

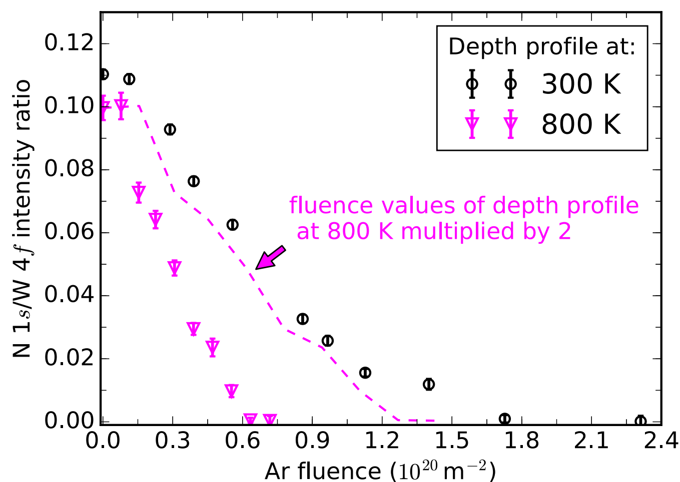

Fig. 9. N Release by Ar irradiation: A W sample was implanted with N at 300 K, subsequently heated to 800 K and then sputtered with Ar ions at elevated temperature. The measured N 1*s* to W 4*f* intensity ratios (triangles) decrease by more than a factor of two faster (dashed line) compared with the N 1*s* to W 4*f* intensity ratios of Ar irradiation at 300 K (circles).

4. Summary

In this study a quantitative analysis of the N accumulation in W and the N release from W_xN by ion irradiation in the temperature range from 300 K to 800 K was conducted. In a laboratory experiment with in-situ heating and XPS analysis capability N_2^+ ions of 300 eV kinetic energy per atom were implanted into a W sample under ultra-high vacuum conditions using a mass-filtered ion source. Sputter depth profiles employing Ar ions of 1keV kinetic energy were measured. In order to determine the N depth distribution, the sputter depth profiles were compared to SDTrimSP simulations, which were, by means of a forward model, converted into depth profiles.

In agreement with [4] and [5] it was found that the formed W_xN does not decompose up to 800 K. However, XPS measurements of N implantation at different implantation temperatures show that the steady-state N 1*s* to W 4*f* intensity ratio decreases approximately linearly with increasing implantation temperature. These observations do not support the thermodynamic calculations in [3], which predict a phase change at 600 K. Additional sputter depth profiles reveal that N does not diffuse into larger depth of the sample. A comparison of measured sputter depth profiles with simulated depth profiles leads to the conclusion that the N concentration in the implantation range of about 2 nm decreases with implantation temperature from 50% at 300 K to 40% at 500 K and to 20% at 800 K.

High resolution measurements show that the N 1*s* signal consists of one peak at 800 K, but a second peak at higher BEs occurs at 600 K which increases further with decreasing implantation temperature. The occurrence of the second peak must be due to a different local atomic arrangement of N in W and could indicate the co-existence of two different W_xN phases at implantation temperatures below 600 K. In measurements where a W_xN sample was irradiated with two different ion species at elevated temperatures, it was found that ion irradiation is needed to induce N release from the W_xN sample already below 800 K. This irradiation-induced N release is strongly temperature-dependent and leads to a decrease of retained N in W by a factor of about 2 when increasing the implantation temperature from 300 K to 800 K.

Acknowledgements

The authors would like to thank colleagues from the IPP, especially Dr. Klaus Schmid for the discussions on the interpretation of the experimental data and Gabriele Matern for preparing the tungsten

samples. This work has been carried out within the framework of the EUROfusion Consortium and has received funding from the Euratom research and training programme 2014–2018 under grant agreement No 633053. The views and opinions expressed herein do not necessarily reflect those of the European Commission. The work was partially carried out under WP PFC.

References

[1] G. Federici, C. Skinner, J. Brooks, J. Coad, C. Grisolia, A. Haasz, A. Hassanein, V. Philipps, C. Pitcher, J. Roth, W. Wampler, D. Whyte, Plasma-material interactions in current tokamaks and their implications for next step fusion reactors, Nucl. Fusion 41 (12) (2001) 1967. http://stacks.iop.org/0029-5515/41/i=12/a=218
[2] A. Kallenbach, M. Bernert, R. Dux, L. Casali, T. Eich, L. Giannone, A. Herrmann, R.M. Dermott, A. Mlynek, H.W. Müller, F. Reimold, J. Schweinzer, M. Sertoli, G. Tardini, W. Treutterer, E. Viezzer, R. Wenninger, M. Wischmeierthe ASDEX Upgrade team, Impurity seeding for tokamak power exhaust: from present devices via ITER to DEMO, Plasma Phys. Controlled Fusion 55 (12) (2013) 124041. http://stacks.iop.org/0741-3335/55/i=12/a=124041
[3] K. Schmid, A. Manhard, C. Linsmeier, A. Wiltner, T. Schwarz-Selinger, W. Jacob, S. Mändl, Interaction of nitrogen plasmas with tungsten, Nucl. Fusion 50 (2) (2010) 025006. http://stacks.iop.org/0029-5515/50/i=2/a=025006
[4] L. Gao, W. Jacob, G. Meisl, T. Schwarz-Selinger, T. Höschen, U. von Toussaint, T. Dürbeck, Interaction of deuterium plasma with sputter-deposited tungsten nitride films, Nucl. Fusion 56 (1) (2016) 016004. http://stacks.iop.org/0029-5515/56/i=1/a=016004
[5] G. Meisl, K. Schmid, O. Encke, T. Höschen, L. Gao, C. Linsmeier, Implantation and erosion of nitrogen in tungsten, New J. Phys. 16 (9) (2014) 093018. http://stacks.iop.org/1367-2630/16/i=9/a=093018
[6] A. Manhard, G. Matern, M. Balden, A step-by-step analysis of the polishing process for tungsten specimens, Practical Metallography 50 (1) (2013) 5–16. https://doi.org/10.3139/147.110215
[7] G. Matthews, Material migration in divertor tokamaks, J. Nucl. Mater. 1–9 (2005) 337–339. http://www.sciencedirect.com/science/article/pii/S0022311504008426
[8] W. Eckstein, Calculated sputtering, reflection and range values, IPP 9/132, Max-Planck-Institut für Plasmaphysik, Garching, 2002. http://hdl.handle.net/11858/00-001M-0000-0027-4522-5
[9] D. Briggs, J. Grant, Surface analysis by Auger and X-ray photoelectron spectroscopy, IM publications, Chichester, 2003. https://books.google.de/books?id=HY6PQgAACAAJ
[10] M. Seah, I. Gilmore, S. Spencer, Quantitative XPS: I. Analysis of X-ray photoelectron intensities from elemental data in a digital photoelectron database, J. Electron Spectros. Relat. Phenomena 120 (1–3) (2001) 93–111, https://doi.org/10.1016/S0368-2048(01)00311-5. http://www.sciencedirect.com/science/article/pii/S0368204801003115
[11] J. Végh, The Shirley background revised, J. Electron Spectros. Relat. Phenomena 151 (3) (2006) 159–164, https://doi.org/10.1016/j.elspec.2005.12.002. http://www.sciencedirect.com/science/article/pii/S0368204805005220
[12] W. von der Linden, V. Dose, U. von Toussaint, Bayesian Probability Theory, Applications in the physical sciences. Cambridge University Press, 2014.
[13] A. Mutzke, R. Schneider, W. Eckstein, R. Dohmen, SDTRimSP version 5.00, IPP 12/8, Max-Planck-Institut für Plasmaphysik, Garching, 2011. http://hdl.handle.net/11858/00-001M-0000-0026-EAFB-6
[14] O. Encke, Wechselwirkung von Stickstoff- und Deuterium-Ionen mit Wolfram, Diploma thesis (in German), Universität Ulm, 2014. http://hdl.handle.net/11858/00-001M-0000-002D-F343-B
[15] J. Scofield, Hartree-Slater subshell photoionization cross-sections at 1254 and 1487 eV, J. Electron Spectros. Relat. Phenomena 8 (2) (1976) 129–137, https://doi.org/10.1016/0368-2048(76)80015-1. http://www.sciencedirect.com/science/article/pii/0368204876800151
[16] J. Yeh, I. Lindau, Atomic subshell photoionization cross sections and asymmetry parameters: $1 \le Z \le 103$, At. Data Nucl. Data Tables 32 (1) (1985) 1–155, https://doi.org/10.1016/0092-640X(85)90016-6. http://www.sciencedirect.com/science/article/pii/0092640X85900166
[17] W. Gries, A universal predictive equation for the inelastic mean free pathlengths of X-ray photoelectrons and Auger electrons, Surf. Interface Anal. 24 (1996) 38.
[18] J. Roth, Chemical erosion of carbon based materials in fusion devices, J. Nucl. Mater. 51–57 (1999) 266–269, https://doi.org/10.1016/S0022-3115(98)00658-8. http://www.sciencedirect.com/science/article/pii/S0022311598006588